The Astrophysical Journal, 879:40 (13pp), 2019 July 1 https://doi.org/10.3847/1538-4357/ab2235

A Search for High-energy Counterparts to Fast Radio Bursts

Virginia Cunningham[1], S. Bradley Cenko[2,3], Eric Burns[2], Adam Goldstein[4], Amy Lien[2], Daniel Kocevski[5], Michael Briggs[6], Valerie Connaughton[4], M. Coleman Miller[1,3], Judith Racusin[2], and Matthew Stanbro[6]
[1] Astronomy Department, University of Maryland, College Park, MD 20742, USA
[2] Astrophysics Science Division, NASA/Goddard Space Flight Center, MC 661, Greenbelt, MD 20771, USA
[3] Joint Space-Science Institute, University of Maryland, College Park, MD 20742-2421, USA
[4] Science and Technology Institute, Universities Space Research Association, Huntsville, AL, USA
[5] Astrophysics Office, ST12, NASA/Marshall Space Flight Center, Huntsville, AL 35812, USA
[6] Department of Space Science, University of Alabama in Huntsville, Huntsville, AL, USA
Received 2019 February 11; revised 2019 May 14; accepted 2019 May 15; published 2019 July 2

Abstract

We report on a search for high-energy counterparts to fast radio bursts (FRBs) with the *Fermi* Gamma-ray Burst Monitor, *Fermi* Large Area Telescope, and the *Neil Gehrels Swift Observatory* Burst Alert Telescope. We find no significant associations for any of the 23 FRBs in our sample, but report upper limits to the high-energy fluence for each on timescales of 0.1, 1, 10, and 100 s. We report lower limits on the ratio of the radio to high-energy fluence, f_r/f_γ, for timescales of 0.1 and 100 s. We discuss the implications of our non-detections on various proposed progenitor models for FRBs, including analogs of giant pulses from the Crab pulsar and hyperflares from magnetars. This work demonstrates the utility of analyses of high-energy data for FRBs in tracking down the nature of these elusive sources.

Key words: gamma rays: general – stars: magnetars – stars: neutron – X-rays: general

1. Introduction

Fast radio bursts (FRBs) are bright (typical fluences of 2 Jy ms), short-duration (few ms) pulses at frequencies of ∼1 GHz (Lorimer et al. 2007; Thornton et al. 2013). FRBs can be distinguished from other short-duration radio pulses (e.g., pulsars) by their high dispersion measures (DMs) for their Galactic latitude (100–2600 pc cm^{-3}; Petroff et al. 2016). Because the DM derived for FRBs can be significantly in excess of the Galactic value (average of ∼250 pc cm^{-3} for Galactic pulsars; Manchester et al. 2005), they must either reside in regions of large overdensities of free electrons if in the Milky Way or at extragalactic distances.

The first FRB was discovered in 2007 (Lorimer et al. 2007) and it was not until 2013 that their reality as a class of astrophysical objects was firmly established (Thornton et al. 2013, see perytons). Only ∼70 FRBs have been published in the literature at the date of this publication (see the FRB Catalog (FRBCAT) at frbcat.org; Petroff et al. 2016). However, because these have been discovered by relatively narrow field-of-view instruments, the true all-sky rate is remarkable: ∼6000 sky^{-1} day^{-1} above a fluence of ∼few Jy ms at ∼1 GHz (Keane & Petroff 2015; Champion et al. 2016; Nicholl et al. 2017). For comparison, this is much larger than the all-sky rate of gamma-ray bursts (∼few per day at current detector sensitivities) and comparable to the rate of supernovae (core-collapse and thermonuclear) out to a redshift of $z \approx 0.5$ (Li et al. 2011).

Only two FRBs are known to exist as repeating bursts: FRB 121102 ("The Repeater") and FRB 180814.J0422+73 (Spitler et al. 2016; The CHIME/FRB Collaboration 2019). FRB 180814.J0422+73 was reported as this work was being completed, so it is not included in our following analysis. Spitler et al. (2016) reported the detection of 12 bursts from the Repeater at 1.4 GHz from Arecibo and 5 bursts at 2 GHz from Green Bank, Chatterjee et al. (2017) reported 9 bursts at 3 GHz from the Very Large Array (VLA), and Scholz et al. (2017) reported 8 bursts at 2 GHz from Green Bank, 2 bursts at 1380 MHz from Arecibo, and 2 bursts seen by both telescopes. All repeating bursts display a consistent DM but can vary in pulse shape and spectral shape. The Repeater exhibits no evidence for periodicity, but instead appears to show episodes of enhanced activity (i.e., active and quiescent periods). Other FRBs have been reobserved, but none show repeated bursting like that displayed by the two previously mentioned FRBs. In several cases it is possible to rule out repeat outbursts with the intensity and frequency of FRB 121102; however, less frequent and/or fainter, repeated outbursts remain viable (Palaniswamy et al. 2018). It is therefore not currently known if all FRBs repeat, or if the known population comprises multiple classes of events (e.g., repeaters and non-repeaters).

Only the repeating FRB 121102 has been localized to within a host galaxy. No obvious host has yet been identified for FRB 180814.J0422+73. Chatterjee et al. (2017) use high angular resolution radio interferometry to place FRB 121102 within a dwarf galaxy at $z \sim 0.2$ (Tendulkar et al. 2017; Yamasuki et al. 2016). The FRB location is consistent with a faint, persistent radio source of unknown origin (Chatterjee et al. 2017). While this result provides unprecedented insight into the physics of the repeating FRB, without detections from radio interferometers for the other FRBs it is impossible to localize them to such high precision using this method.

Despite being a recent discovery, FRBs have nonetheless piqued great interest in the area of high-time-resolution radio astronomy. This excitement can be divided into two separate motivations: FRBs may become powerful probes of the intergalactic medium (IGM), and the emission mechanism powering these outbursts may help clarify some long-standing issues in astrophysics, including the missing baryon problem and the nature of coherent emission (see below).

The large DMs derived from FRBs suggest that the signals have encountered more free electrons than can be accounted for in the ISM of the Milky Way. While Galactic models resulting from a large local density of free electrons do exist (e.g., Maoz et al. 2015), the most natural explanation is that FRBs are of

extragalactic origin (e.g., Thornton et al. 2013). In fact if all the DM were to result from electrons in the IGM, this would imply cosmological redshifts of $z \approx 0.5$–1.0 for these events.

The possibility of using FRBs to measure the density of free electrons at cosmological distances may offer a way to solve the "missing baryons" problem. In the local universe, only half of cosmic baryons reside at densities and temperatures that result in detectable emission and/or absorption (Bregman 2007; Shull et al. 2012). McQuinn (2014) demonstrated how the location of these baryons can be inferred from the distribution of DM (at a fixed redshift). Similarly, samples extending out to $z \approx 3$ with measured DM and redshift may even be able to constrain the equation of state of dark energy (Zhou et al. 2014).

In addition to their potential utility as cosmological probes, FRBs also offer a means to improve our understanding of coherent emission processes. Any source emitting incoherently (e.g., synchrotron radiation) cannot exceed a brightness temperature of 10^{12} K (Readhead 1994). For a typical FRB with an intrinsic duration of 1 ms, causality limits the size of the emitting region to be less than 300 km barring bulk relativistic motion. For FRBs at distances of $\sim$1 Gpc, the peak flux densities of $\sim$1 Jy at $\nu \sim 1$ GHz imply a brightness temperature of $T_B \gtrsim 10^{35}$ K. Clearly, for FRBs $T_B \gg 10^{12}$ K, from which we infer that FRBs must be emitting coherent radiation. Only a handful of astronomical sources are known to radiate coherently, with pulsars being the most well-known example. Given the large uncertainties in the pulsar emission mechanism, the advent of FRBs offers the real hope of fundamental progress toward understanding coherent processes in this long-standing field.

As with many astronomical phenomena, the number of theoretical models has rapidly grown larger than the number of known FRBs. Here, we consider several of the more plausible models, which must incorporate the following basic tenets: compact emission region, extragalactic distance scale, coherent emission mechanism, repeated outbursts from at least some FRBs, and large all-sky rates. We consider models for FRBs resulting from outbursting neutron stars (either magnetically or rotationally powered), as mergers between neutron star binaries, or as "cosmic combs." We describe the models and their various predictions in greater detail in Section 3.

The goal of this paper is to search for possible counterparts at high-energy wavelengths to FRBs. We use data from the *Fermi* Gamma-ray Burst Monitor (GBM; Meegan et al. 2009), the *Fermi* Large Area Telescope (LAT; Atwood et al. 2009), and the *Neil Gehrels Swift Observatory* (Gehrels et al. 2004) Burst Alert Telescope (BAT; Barthelmy et al. 2005) to search for X-ray and gamma-ray (8 keV–300 GeV) counterparts to FRBs. Although the energy range of the *Swift* BAT overlaps with the *Fermi* GBM, we choose to include the BAT due to its arcminute localization, compared to the GBM. Scholz et al. (2016) used the same instruments to search for sources related to the repeating FRB but report no significant detections. They conducted another campaign coordinating observations between the Green Bank, Effelsberg, and Arecibo radio telescopes and the *Chandra X-ray Observatory* and *XMM-Newton* (Scholz et al. 2017; this has been noted again in the reference section) but also report no significant X-ray detections. Their searches focus on a single FRB but our project extends to cover all FRBs within the field of view of each instrument as well as extending the timescales of interest that were analyzed. One advantage of this population study is the ability to potentially identify fundamental differences between repeating and non-repeating FRBs. There also exist upper limits for three FRBs from the *International Gamma-Ray Astrophysics Laboratory* observatory (Savchenko et al. 2018a, 2018b, 2018c), which has comparable energy coverage to the *Fermi* GBM and *Swift* BAT. These limits are in agreement with the limits found here in this paper.

Tendulkar et al. (2016) placed limits on the ratio of radio to gamma-ray emission for FRBs based on observations of SGR 1806−20. We conduct a more sensitive search for high-energy counterparts in the GBM by employing the targeted search techniques developed for coincident searches for gravitational-wave counterparts (Blackburn et al. 2015). We also use these ratios to compare our results with the proposed gamma-ray counterpart to FRB 131104 (DeLaunay et al. 2016). With the exception of the host galaxy for FRB 121102 (Chatterjee et al. 2017; Marcote et al. 2017; Tendulkar et al. 2017), no other electromagnetic analogs have so far been confirmed, despite rigorous efforts.

The detection of robust high-energy signals from FRBs would have a significant impact on the field, as current theories predict widely differing high-energy fluences. Although a confirmed, positive detection of a high-energy counterpart would definitively rule out many theories, a non-detection and corresponding upper limit could also eliminate many as well.

This paper is organized as follows. In Section 2 we describe the data products and analysis methods for calculating the high-energy upper limits for each FRB. In Section 3 we compare our results with various theories from the literature before we draw our conclusions in Section 4 on the likelihood and implications for each model. In this work we assume a standard ΛCDM cosmology and that the Milky Way is well-described by Galactic structure models such as NE2001 (Cordes & Lazio 2002).

2. Data and Results

There are 23 published FRBs used in this analysis (taken from the FRBCAT) as of 2017 July. Seventeen FRBs were detected with the Parkes Radio Telescope, three with UTMOST (Upgrade of The Molonglo Observatory Synthesis Telescope), one with the Arecibo Telescope, one with the Green Bank Telescope, and one with ASKAP (the Australian Square Kilometre Array Pathfinder). We search for contemporaneous high-energy emission from all these events with three different instruments: *Fermi* GBM, *Fermi* LAT, and *Swift* BAT (see Table 3 in the Appendix for a breakdown of available observations per FRB). We search for high-energy emission on a variety of different timescales. To place limits on a coincident (i.e., ms-long) pulse, we utilize the smallest time bin available from each relevant instrument. Where possible, we also place limits on timescales[7] of 0–1, 0–10, and 0–100 s. This spans the range from hyperflares of magnetars ($\Delta t \sim 0.1$ s) to short ($\Delta t \sim 1$ s) and long ($\Delta t \sim 10$–100 s) gamma-ray bursts (GRBs).

2.1. Fermi *GBM*

The GBM (Meegan et al. 2009) is a collection of hard X-ray/soft gamma-ray detectors on board the *Fermi Gamma-ray Space Telescope* sensitive to photons with energies from

[7] We take the zero-point time, $t_{\rm frb}$, as the arrival time of an infinite energy photon.

8 keV to 40 MeV. *Fermi* is in a low-Earth (96 minutes) orbit, and the GBM is sensitive to gamma-rays from the entire sky unocculted by Earth when outside the South Atlantic Anomaly (SAA).

The GBM consists of two sets of detectors: 12 sodium iodide (NaI) scintillators cover a lower energy range from 8 keV to 1 MeV, and 2 bismuth germanate (BGO) scintillators cover the higher end from 300 keV to 40 MeV. The 12 NaI detectors are positioned to enable all-sky coverage, while the 2 omnidirectional BGO detectors are positioned on opposite sides of the spacecraft for the same reason. The 14 detectors are positioned in such a way that any burst should be seen by multiple detectors. The 12 NaI detectors are used for triggering and localization and the two BGO enable a broader energy range for spectroscopy. The rates received by each detector combined with their relative position and angle to each other allow the position of bursts to be determined to a few degrees accuracy (Connaughton et al. 2015).

Each of the 14 detectors in the GBM records several data products. The two of interest for this work are continuous time (CTIME) and time-tagged events (TTE). The CTIME data are binned by 0.256 s with eight energy channels. The TTE data are continuous event data precise to 2 μs with 128 energy channels. Due to the short duration of FRBs, TTE data are preferred over CTIME; however, continuous TTE data only started in 2012, so they are not available for every FRB in our sample.

Of the 23 FRBs in our sample, 20 occurred after *Fermi*'s launch. Of those 20, 12 were visible to *Fermi* during good time intervals for GBM. Of the 38 repeat bursts of FRB 121102, 15 were visible to *Fermi* during good time intervals for GBM. To determine if a candidate counterpart exists in GBM data we ran a targeted search (Blackburn et al. 2015; Goldstein et al. 2016) of GBM data around $t_{\rm FRB}$ for $\pm$15 s for the 0.1 and 1.0 s timescales, $\pm$250 s for the 10 s timescales, and $\pm$400 s for the 100 s timescales (the 100 s timescale was only searched when the background was stable over periods of a few hundred seconds and had continuous TTE coverage).

The targeted search was designed to identify untriggered, faint, short GRB-like counterparts to gravitational-wave events, which makes it a useful tool to adapt to our purposes. We use the same three standard spectral templates described in Goldstein et al. (2016), which generally cover the diverse range of short to long GRBs: a low-energy soft Band function (Band et al. 1993; $E_{\rm peak} = 70$ keV), a medium-energy Band function ($E_{\rm peak} = 230$ keV), and a power law with an exponential cutoff ($E_{\rm peak} = 1.5$ MeV). While we calculate fluence upper limits for each of these three spectral types, the limits listed in this paper will be given for the hardest template. On average, this harder spectral template results in a factor of $\sim$2.5 times the fluence of the medium-energy template and $\sim$5 times the fluence of the low-energy template.

We employ the Bayesian likelihood analysis originally developed by Blackburn et al. (2015) to search for contemporaneous signals around the FRB radio detections. This method calculates the likelihood of a signal matching one of the three spectral templates compared to the null hypothesis of a constant background. Owing to the highly transient universe in the gamma-ray band and GBM's all-sky coverage there were a few real transient gamma-ray signals in GBM during time intervals of interest; however, these are known to be unrelated due to inconsistent sky localizations or classification as a known source type (e.g., a solar flare). No possibly related signal is significant over the total lifetime of the search (see the Appendix for more details on these unrelated signals).

In the absence of any correlated gamma-ray signal with the FRBs, we estimate flux upper limits in the search time windows around each $t_{\rm FRB}$ on timescales of 0.1, 1, 10, and 100 s using the same spectral templates that were used by the targeted search. These conservative upper limits were calculated by utilizing the NaI detector with the smallest normal angle to the FRB, and estimating the maximum 3σ count rate flux upper limit in the window based on the modeled background noise. The count rate upper limit was then converted to a flux upper limit by assuming each of the template spectra, folding them through the GBM detector responses calculated for the FRB sky location, and fitting for the amplitude of the template spectra. This procedure results in 3σ flux upper limits listed in Table 1. Five of these FRBs are analyzed by Tendulkar et al. (2016), where the limiting gamma-ray fluence is estimated to be 1×10^{-8} erg cm^{-2}, roughly consistent with the faintest known short GRBs detected by GBM. The targeted search used here provides consistent, though slightly shallower, limits to Tendulkar et al. (2016).

In addition, we consider the results derived from performing a stacking analysis of the bursts from the Repeater and a separate stacking analysis of the bursts from the non-repeating FRBs. In the case of the non-repeating FRBs we assume that all FRBs are approximately at the same redshift ($z = 0.1$–0.3). This assumption will be justified in Section 3, where each of the models we consider in this work limits the distance of the FRBs to no further than $\sim$1 Gpc. We find no obvious potential signals that would warrant any further stacking analysis for either case.

2.2. Fermi *LAT*

The LAT (Atwood et al. 2009) is a pair-conversion telescope on board the *Fermi* satellite, sensitive to gamma-rays with energies between 20 MeV and more than 300 GeV. The LAT has a wide field of view (FOV), scans continuously and covers approximately 20% of the sky at any given time. The LAT completes all-sky coverage every two orbits over a duration of about three hours. The timing accuracy of the LAT is better than 10 μs and its localization precision is highly energy-dependent ($\sim 5'$ for GeV photons).

We search the *Fermi* LAT data for gamma-ray counterparts by performing an unbinned likelihood analysis using the standard analysis tools developed by the LAT team (ScienceTools version v10r01p0).[8] For this analysis, we use the "P8R2_TRANSIENT_V6" instrument response functions and select "Transient" class events in the 0.1–100 GeV energy range from a 12° radius energy-independent region of interest (ROI) centered on the FRB location. The size of the ROI is chosen to reflect the 95% containment radius of the LAT energy-dependent point-spread function at 100 MeV. The "Transient" event class is chosen because it represents looser cuts against non-photon background contamination and is typically used to study GRBs on very short timescales (Ackermann et al. 2012).

In standard unbinned likelihood analysis, the observed distribution of counts at a particular position is fit to a model that includes all known gamma-ray sources in the 3FGL

[8] http://fermi.gsfc.nasa.gov/ssc/

Table 1
3σ Upper Limits to f_γ in Different Time Ranges and Energy Bands for Each FRB

FRB Name	Bandpass	Date (yyyy mm dd)	Time (hh:mm:ss)	R.A.	Decl.	Δt (s)	f_γ[a] (10^{-6} erg cm^{-2})
090625	8 keV–40 MeV	2009 Jun 25	21:53:51	46.95	−29.93	100	<7.9
						10	<2.5
						1	<0.82
						0.1	<0.28
110523	8 keV–40 MeV	2011 May 23	15:06:20	326.30	−0.16	100	<7.5
						10	<2.3
						1	<0.76
						0.1	<0.26
110626	8 keV–40 MeV	2011 Jun 26	21:33:16	315.75	−44.73	100	<7.5
						10	<2.3
						1	<0.76
						0.1	<0.26
110703	8 keV–40 MeV	2011 Jul 3	18:59:39	352.50	−2.87	100	<8.2
						10	<2.6
						1	<0.84
						0.1	<0.29
130628	8 keV–40 MeV	2013 Jun 28	03:57:59	135.76	3.44	100	<6.6
						10	<2.1
						1	<0.7
						0.1	<0.24
130729	8 keV–40 MeV	2013 Jul 29	09:01:51	205.34	−6.00	100	<7.1
						10	<2.3
						1	<0.75
						0.1	<0.26
131104	8 keV–40 MeV	2013 Nov 4	18:04:00	101.04	−51.28	100	<8.4
						10	<2.7
						1	<0.87
						0.1	<0.3
150215	8 keV–40 MeV	2015 Feb 15	20:41:39	274.36	−4.90	100	<7.0
						10	<2.2
						1	<0.73
						0.1	<0.25
150418	8 keV–40 MeV	2015 Apr 18	04:29:05	109.12	−19.04	100	<7.1
						10	<2.3
						1	<0.74
						0.1	<0.25
150807	8 keV–40 MeV	2015 Aug 7	17:53:55	340.10	−55.27	100	<6.9
						10	<2.2
						1	<0.73
						0.1	<0.25
160317	8 keV–40 MeV	2016 Mar 17	09:00:30	118.45	−29.61	100	<7.0
						10	<2.2
						1	<0.73
						0.1	<0.25
160608	8 keV–40 MeV	2016 Jun 8	03:52:57	114.17	−40.80	100	<7.7
						10	<2.4
						1	<0.79
						0.1	<0.27
121102 3	8 keV–40 MeV	2015 May 17	17:51:41	82.99	33.15	100	<7.6
						10	<2.4
						1	<0.78
						0.1	<0.26
121102 4	8 keV–40 MeV	2015 Jun 2	16:38:08	82.99	33.15	100	<6.5
						10	<2.1
						1	<0.69
						0.1	<0.24
121102 5	8 keV–40 MeV	2015 Jun 2	16:47:36	82.99	33.15	100	<6.7
						10	<2.1
						1	<0.69
						0.1	<0.24
121102 17	8 keV–40 MeV	2015 Dec 8	04:54:40	82.99	33.15	100	<7.2
						10	<2.3
						1	<0.75

Table 1
(Continued)

FRB Name	Bandpass	Date (yyyy mm dd)	Time (hh:mm:ss)	R.A.	Decl.	Δt (s)	f_γ[a] (10^{-6} erg cm^{-2})
						0.1	<0.25
121102 18	8 keV–40 MeV	2016 Aug 23	17:51:24	82.99	33.15	100	<7.6
						10	<2.4
						1	<0.79
						0.1	<0.26
121102 19	8 keV–40 MeV	2016 Sep 2	16:19:00	82.99	33.15	100	<7.2
						10	<2.3
						1	<0.76
						0.1	<0.26
121102 20	8 keV–40 MeV	2016 Sep 2	16:41:02	82.99	33.15	100	<7.7
						10	<2.4
						1	<0.79
						0.1	<0.27
121102 21	8 keV–40 MeV	2016 Sep 7	11:59:06	82.99	33.15	100	<8
						10	<2.6
						1	<0.84
						0.1	<0.29
121102 22	8 keV–40 MeV	2016 Sep 12	10:58:31	82.99	33.15	100	<7.3
						10	<2.4
						1	<0.78
						0.1	<0.26
121102 24	8 keV–40 MeV	2016 Sep 15	11:11:03	82.99	33.15	100	<7.5
						10	<2.4
						1	<0.78
						0.1	<0.27
121102 27	8 keV–40 MeV	2016 Sep 17	10:29:09	82.99	33.15	100	<7
						10	<2.2
						1	<0.73
						0.1	<0.25
121102 28	8 keV–40 MeV	2016 Sep 18	04:10:17	82.99	33.15	100	<8
						10	<2.5
						1	<0.83
						0.1	<0.28
121102 29	8 keV–40 MeV	2016 Sep 18	05:14:14	82.99	33.15	100	<8.5
						10	<2.7
						1	<0.89
						0.1	<0.3
121102 33	8 keV–40 MeV	2017 Jan 12	01:39:26	82.99	33.15	100	<7.2
						10	<2.3
						1	<0.76
						0.1	<0.26
121102 34	8 keV–40 MeV	2017 Jan 12	02:25:12	82.99	33.15	100	<6.6
						10	<2.1
						1	<0.69
						0.1	<0.24
121102 35	8 keV–40 MeV	2017 Jan 12	02:36:30	82.99	33.15	100	<6.8
						10	<2.2
						1	<0.72
						0.1	<0.25
121102 37	8 keV–40 MeV	2017 Jan 12	03:16:33	82.99	33.15	100	<6.8
						10	<2.2
						1	<0.71
						0.1	<0.24
121102 38	8 keV–40 MeV	2017 Jan 12	03:26:24	82.99	33.15	100	<7.5
						10	<2.3
						1	<0.75
						0.1	<0.25
090625	60 MeV–100 GeV	2009 Jun 25	21:53:51	46.95	−29.93	100	<0.31
130628	60 MeV–100 GeV	2013 Jun 28	03:57:59	135.76	3.44	100	<0.83
150215	60 MeV–100 GeV	2015 Feb 15	20:41:39	274.36	−4.90	100	<1.5
150418	60 MeV–100 GeV	2015 Apr 18	04:29:05	109.12	−19.04	100	<0.31
160317	60 MeV–100 GeV	2016 Mar 17	09:00:30	118.45	−29.61	100	<0.77
160608	60 MeV–100 GeV	2016 Jun 8	03:52:57	114.17	−40.80	100	<0.38

Table 1
(Continued)

FRB Name	Bandpass	Date (yyyy mm dd)	Time (hh:mm:ss)	R.A.	Decl.	Δt (s)	f_γ[a] (10^{-6} erg cm^{-2})
121102 18	60 MeV–100 GeV	2016 Aug 23	17:51:24	82.99	33.15	100	<0.45
121102 19	60 MeV–100 GeV	2016 Sep 2	16:19:00	82.99	33.15	100	<1.4
121102 22	60 MeV–100 GeV	2016 Sep 12	10:58:31	82.99	33.15	100	<0.73
121102 27	60 MeV–100 GeV	2016 Sep 17	10:29:09	82.99	33.15	100	<0.5
121102 34	60 MeV–100 GeV	2017 Jan 12	02:25:12	82.99	33.15	100	<1.4
110626	15–350 keV	2011 Jun 26	21:33:16	315.75	−44.73	300	<4.8
150215	15–350 keV	2015 Feb 15	20:41:39	274.36	−4.90	300	<2.3
						100	<0.065
						10	<0.055
						1	<0.027
						0.064	<0.0092
160410	15–350 keV	2016 Apr 10	08:33:38	130.35	6.08	300	<1.6
						100	<0.17
						10	<0.08
						1	<0.021
						0.064	<0.0048

Note.
[a] Values listed here are the fluence for the spectral template of a power law with an exponential cutoff ($E_{\rm peak}$ = 1.5 MeV). We also explore two softer spectral templates. See Section 2.1 for more information.

catalog (Acero et al. 2015) within a radius of 30°, as well as Galactic and isotropic background components.[9] The Galactic component, *gll_iem_v06*, is a spatial and spectral template that accounts for interstellar diffuse gamma-ray emission from the Milky Way. The isotropic component, *iso_transient_v06*, provides a spectral template to account for all remaining isotropic emission, including contributions from both residual charged particle backgrounds and the isotropic celestial gamma-ray emission. Possible emission from a FRB is modeled as an uncataloged point source with a power-law spectrum where the normalization and photon index are left as free parameters. A likelihood-ratio test is then employed to quantify whether there exists a significant excess of counts due to the uncataloged point source above the expected background model. If no significant new source is found, we calculate the 95% confidence level upper limits using a Bayesian method described in Ackermann et al. (2016), which we convert to a fluence limit for the relevant timescale. Note that these fluence limits are calculated via a different method than we use for the GBM (Section 2.1) and BAT (Section 2.3) data.

The three earliest FRBs are again excluded from our analysis because they occurred before *Fermi* was launched on 2008 June 11. Of the remaining 19 non-repeating FRBs, 6 are located within the LAT FOV at the time of radio detection. Of the 38 repeating bursts, 5 are in the LAT FOV as well. We examine two time intervals based on the zero-point detection time, $t_{\rm FRB}$: 0–10 and 0–100 s (Table 1). No photons are detected for any of the FRBs within 1 s of the initial burst.

2.3. Swift *BAT*

The *Neil Gehrels Swift Observatory* (Gehrels et al. 2004) BAT is a coded-aperture instrument dedicated to triggered hard X-ray observations of GRBs. The BAT detectors have an energy range of 15–300 keV with a resolution of ∼7 keV, a large FOV of 1.4 steradians (half-coded) and a positional accuracy of ∼3′ (Barthelmy et al. 2005). Although the detectors are sensitive up to 300 keV, the coded mask is transparent to photons above 150 keV and so is unable to determine their direction from the sky. When running in survey mode, BAT collects detector plane histograms that are binned in ∼300 s. These detector plane histograms can be used to generate sky images and search for sources in the BAT FOV. In addition to these spatially resolved images, BAT also collects raw rate data from all of the enabled detectors. The raw rate data are a continuous stream of events that can be used to search for GRB triggers not in the BAT FOV. We analyze both the five-minute time-binned survey images and the 64 ms-binned, four energy band (15–25, 25–50, 50–100, and 100–350 keV) rate data light curves using the standard *Swift*-specific tools provided by the HEASoft package (version 6.18).

Only FRB 110626, FRB 150215, and FRB 160410 were within the BAT FOV at the time of radio detection. The three earliest FRBs occurred prior to *Swift*'s launch on 2004 November 20, so they are excluded from the analysis. Of the 19 non-repeating FRBs examined 10 of the bursts were out of the FOV, and one did not occur during recorded observations (i.e., the telescope was most likely slewing to a new location), 3 were within the FOV while the BAT was in the SAA, and 1 occurred while the BAT was slewing. Of the 38 repeating signals from FRB 121102, 30 were not within the FOV at the time of detection and 6 occurred while the BAT was in the SAA. Three of the bursts (FRB 131104 and bursts two and three of FRB 121102) were located right on the edge of the BAT FOV but are excluded from analysis due to their low partial coding fraction. It is standard practice[10] to remove pointings with partial coding fractions corresponding to less than 10% of the array being illuminated (Krimm et al. 2013).

The survey images provide more accurate positional information compared to the rate data. The rate data are the cumulative sum of all counts seen within and around the BAT FOV. It can be difficult to definitively attribute a significant rise

[9] https://fermi.gsfc.nasa.gov/ssc/data/access/lat/BackgroundModels.html

[10] DeLaunay et al. (2016) reported a *Swift* BAT counterpart to FRB 131104 with a partial coding fraction of 2.9%. A more detailed analysis of this event is currently underway for a separate work (Sakamoto et al. 2019, in preparation).

in counts to any single FRB, as it could also be due to a nearby source. In the survey images the precise timing information is lost due to the 300 s binning of the counts. While the rate data are useful for identifying sudden significant changes in the aggregate background emission on short timescales, the survey images are more accurate for producing limits for the specific FRB locations. The fluence limits derived from the rate data are shallower than, yet still consistent with, the limits derived from the survey images.

We find no significant counterpart detections at the 3σ confidence level for FRB 110626, FRB 150215, and FRB 160410, but we are able to determine upper limits to the high-energy fluence. We produce 8-channel spectra using the mask-weighted background variation counts detected in the survey images, and estimate the flux that would have been equivalent to a 3σ detection. Assuming a simple power-law function with an index of 2.0 for the FRB spectra, we calculate an estimate of the flux within XSPEC based on the spectral fit over an energy range of 15–350 keV (Arnaud 1996). We use the FRB location on the BAT FOV to generate the instrument response matrix corresponding to the respective grid ID on the BAT detector (Lien et al. 2014). The fluence limits are listed in Table 1 for 300 s timescales. Here we find comparable limits for those same FRBs analyzed by Tendulkar et al. (2016) with *Swift* BAT.

For comparison we also examine the raw rate data for FRB 150215 and FRB 160410.[11] We model the rate background emission over a total of 500 s as a linear fit in time. If necessary we use a low-order polynomial fit instead. We compute the root mean square of the background level in 200 s duration bins at ± 50 s from the time region of interest and denote the total number of counts in the bins as $N_{\rm bins}$. We assume that the scatter within the region of interest also follows this scatter as well. From there we calculate 3σ upper limits on the count rate assuming Poisson statistics. We then use XSPEC to convert the count rate limit to a fluence over the same energy range as the survey data. We find consistent results between the event rate data and survey images.

3. Analysis and Interpretation

We report no significant excess in high-energy emission from the *Fermi* GBM, *Fermi* LAT, or *Swift* BAT for any of the individual FRBs or repeats from FRB 121102. The expected high-energy fluence from FRBs is highly model-dependent. Given the number of theories in the literature we take a two-fold approach in this work. First, we compare our results with previously reported observations of high-energy counterparts to FRBs, such as that claimed for FRB 131104. Second, we consider the implications of our non-detections for some of the more plausible models that have been considered.

3.1. Limits on the Ratio of Radio to Gamma-Ray Fluence

A recent paper by DeLaunay et al. (2016) reports a possible connection of FRB 131104 to a *Swift* BAT long GRB with fluence $f_\gamma \approx 4 \times 10^{-6}$ erg cm^{-2} and duration $T_{90} = 377$ s, where T_{90} is defined as the time over which a burst emits from 5% of its total measured counts to 95%. With the reported radio fluence for FRB 131104 of 2.33 Jy ms, this implies a ratio of radio to gamma-ray emission of $\approx 6 \times 10^5$ Jy ms erg^{-1} cm^2. For consistency with the DeLaunay result we consider fluences on 100 s timescales. The radio fluences are taken from the FRBCAT. We find that $f_r/f_\gamma \gtrsim 10^5$–$10^7$ Jy ms erg^{-1} cm^2 for the non-repeating FRBs in our sample and we find $f_r/f_\gamma \gtrsim 10^4$–$10^5$ Jy ms erg^{-1} cm^2 for the repeating bursts of FRB 121102 (Table 2). None of the limits derived from the *Swift* BAT or *Fermi* LAT are consistent with the DeLaunay result, providing lower limits to the radio to gamma-ray emission ratio that exceed their reported values. However, 9 out of the 11 non-repeating FRBs and all of the repeating bursts from the *Fermi* GBM are consistent.

We then compare our limits to those expected from magnetar hyperflares (see Section 3.2.2), given observations of SGR 1806−20. Tendulkar et al. (2016) found upper limits of $f_r/f_\gamma < 10^7$ Jy ms erg^{-1} cm^2 for the giant flare event on 2004 December 27, based on archival observations of FRBs taken with the Konus-*Wind* gamma-ray spectrometer, the *Swift* BAT, and the *Fermi* GBM. Although the timescales and the bandpass of Konus-*Wind* (10 keV–10 MeV) are not identical to our analysis, this is inconsistent with four of the non-repeating FRBs yet consistent with all of the repeating bursts (10 in our sample) for limits on timescales of order 0.1 s (Table 2).

We also compare our ratios to those of Scholz et al. (2017), who found a lower limit on f_r/f_γ of $>2 \times 10^8$ based on *Fermi* GBM observations of the Repeater. Although they look at bursts on finer timescales of a few hundred milliseconds, this is consistent with all of our *Fermi* GBM limits on timescales of 0.1 s.

3.2. Constraints on Theoretical Models

Given that there are dozens of theories put forth attempting to explain FRBs, because of their implied small sizes (<300 km), we choose to favor models involving compact objects like neutron stars. We cannot examine all models in our analysis here so we consider only those models that satisfy the criteria of a compact emission region, extragalactic distance scale, coherent emission mechanism, repeated outbursts from at least some FRBs, and large all-sky rates. Here we consider the ramifications of our results in reference to some of the more probable theories.

3.2.1. Rotationally Powered Pulses from Neutron Stars

The Crab pulsar exhibits rare, giant radio pulse behavior at GHz frequencies. Giant pulse occurrences are random in time but are correlated with the pulsar's main pulse or interpulse periods. About 1% of pulses from the Crab are giant pulses. These giant bursts can exceed 0.5 MJy over a duration of a few nanoseconds (Cordes & Wasserman 2016). The most extreme event was a 0.4 ns pulse with a flux density of 2.2 MJy at 9 GHz (Hankins & Eilek 2007). The short durations, large fluxes, and non-periodic nature of giant pulses make them an excellent test for comparison with FRBs.

The Crab emits across all frequencies and also exhibits giant pulse behavior in the gamma- and X-ray as well (Bühler & Blandford 2014). Mickaliger et al. (2012) examine the correlation between radio giant pulses and high-energy photons from 0.1 to 100 GeV and find no significant association.

If FRBs are powered by giant pulses from pulsars then we would expect them to be nearby. Cordes & Wasserman (2016) showed that even the most extreme giant pulse from the Crab could not provide the necessary radio fluences of ~2 Jy ms at 1 Gpc (the reported distance of the Repeater). For these

[11] A flare from a nearby X-ray binary occurred at the same time as FRB 110626, so we exclude those results for the rate data here.

Table 2
Maximum 3σ Ratio of Radio to High-energy Emission on 100 and 0.1 s Timescales

FRB Name	Bandpass	Δt (s)	f_r (Jy ms)	f_γ (10^{-6} erg cm^{-2})	$\log(f_r/f_\gamma)$ (Jy ms erg^{-1} cm^2)
090625	8-4e4 keV	100	2.19	<7.9	>5.44
		0.1		<0.28	>6.89
110523	8-4e4 keV	100	1.04	<7.5	>5.14
		0.1		<0.26	>6.60
110626	8-4e4 keV	100	0.56	<7.5	>4.88
		0.1		<0.26	>6.33
110703	8-4e4 keV	100	1.80	<8.2	>5.34
		0.1		<0.29	>6.80
130628	8-4e4 keV	100	1.22	<6.6	>5.26
		0.1		<0.24	>6.70
130729	8-4e4 keV	100	3.43	<7.1	>5.68
		0.1		<0.26	>7.13
131104	8-4e4 keV	100	2.33	<8.4	>5.45
		0.1		<0.3	>6.89
150215	8-4e4 keV	100	1.96	<7	>5.45
		0.1		<0.25	>6.90
150418	8-4e4 keV	100	1.76	<7.1	>5.39
		0.1		<0.25	>6.84
150807	8-4e4 keV	100	44.80	<6.9	>6.81
		0.1		<0.25	>8.26
160317	8-4e4 keV	100	69.00	<7	>7.00
		0.1		<0.25	>8.44
160608	8-4e4 keV	100	37.00	<7.7	>6.68
		0.1		<0.27	>8.14
121102 3	8-4e4 keV	100	0.10	<7.6	>4.12
		0.1		<0.26	>5.58
121102 4	8-4e4 keV	100	0.20	<6.5	>4.49
		0.1		<0.24	>5.93
121102 5	8-4e4 keV	100	0.09	<6.7	>4.13
		0.1		<0.24	>5.58
121102 17	8-4e4 keV	100	0.09	<7.2	>4.10
		0.1		<0.25	>5.55
121102 28	8-4e4 keV	100	0.36	<8	>4.65
		0.1		<0.28	>6.11
121102 29	8-4e4 keV	100	0.29	<8.5	>4.53
		0.1		<0.3	>5.98
121102 33	8-4e4 keV	100	0.62	<7.2	>4.93
		0.1		<0.26	>6.38
121102 35	8-4e4 keV	100	0.03	<6.8	>3.65
		0.1		<0.25	>5.09
121102 37	8-4e4 keV	100	0.22	<6.8	>4.51
		0.1		<0.24	>5.96
121102 38	8-4e4 keV	100	0.10	<7.5	>4.13
		0.1		<0.25	>5.60
090625	60-1e5 MeV	100	2.19	<0.31	>6.85
130628	60-1e5 MeV	100	1.22	<0.83	>6.17
150215	60-1e5 MeV	100	1.96	<1.5	>6.10
150418	60-1e5 MeV	100	1.76	<0.31	>6.75
160317	60-1e5 MeV	100	69.00	<0.77	>7.95
160608	60-1e5 MeV	100	37.00	<0.38	>7.99
150215	15–350 keV	100	1.96	<0.065	>7.48
		0.1		<0.0092	>5.60
160410	15–350 keV	100	34.00	<0.17	>8.29
		0.1		<0.0048	>9.85

observed fluences they find a maximum distance for Crab-like giant pulses of ~100 Mpc.

An extremely energetic burst of gamma-rays from the Crab occurred in 2011 April with a luminosity of $L_\gamma = 4 \times 10^{36}$ erg s^{-1} (Striani et al. 2011; Buehler et al. 2012). If we assume this energy scale for FRBs, then at 1 Gpc we would expect to observe a fluence around 20 orders of magnitude fainter than the background level. The expected flux density is orders of magnitude too small at 1 Gpc to account for the radio emission observed. However, if indeed the FRBs are located at these Galactic distances this would imply that most of the DM is local to the source, rather than from the IGM. Although the

distances derived here are inconsistent with that of the Repeater we still consider giant Crab-like pulses as a viable model for FRBs because the energy scale and lack of high-energy emission are consistent with that observed for FRBs.

3.2.2. Magnetically Powered Pulses from Neutron Stars

Magnetars are highly magnetized neutron stars with surface magnetic field strengths of $B_{\rm surf} \sim 10^{14}$–$10^{15}$ G (Duncan & Thompson 1992). They are known to regularly emit hard X-ray/soft gamma-ray flares of duration <1 s with total energy 10^{41} erg (Kouveliotou et al. 1998). Distinct from these "average flares," magnetars can also emit hyperflares that are several orders of magnitude higher in energy. A hyperflare is marked by a millisecond rise time, hard X-ray peak, and an oscillating tail lasting for minutes. Although there are ∼30 magnetars known to date, there are only three observed hyperflare events, with the SGR 1806−20 event being the most energetic (Mazets et al. 1979; Hurley et al. 1999, 2005; Palmer et al. 2005).

Magnetar hyperflares are a popular theory for FRBs (Popov & Postnov 2013; Lyubarsky 2014; Kulkarni et al. 2015; Pen & Connor 2015). They have sub-second time variation, extreme energetics, and (depending on assumptions made about the underlying magnetar population) comparable event rates (Nicholl et al. 2017). Magnetars are thought to be correlated with recent star formation and should therefore be enshrouded in dense gas and dust. This would imply a significant portion of an FRB's DM can be attributed to its local environment, rather than to the IGM, placing them at extragalactic, but not necessarily cosmological distances. The properties of the host galaxy of the repeating FRB (e.g., a low-mass, low-metallicity, star-forming dwarf galaxy at redshift $z \sim 0.2$) is consistent with where we might expect to find magnetars (Tendulkar et al. 2017).

If FRBs are caused by magnetar-like hyperflares we can place constraints on their distances by assuming a similar energy release to the SGR 1806−20 event. The total flare energy of this event is 10^{47} erg and could only have been observed out to 40 Mpc before falling below the threshold of most X-ray/gamma-ray telescopes. Figure 1 shows the inferred E_γ for each FRB at different distances, neglecting k-corrections.[12] We can be conservative and consider possibilities that other hyperflares could be stronger than the SGR 1806−20 event, therefore pushing the maximum energy release to $E_\gamma = 10^{49}$ erg. For fluence upper limits set by the harder spectral template in GBM we find the FRBs should be located no nearer than about 0.5 Gpc, which is consistent with the distance of the Repeater at 1 Gpc.

There are a few caveats with this picture. One is that, based on the SGR 1806−20 event, we may not expect to see any radio emission from these hyperflares (see Section 3.1). On the other hand, Lyutikov (2002) proposed a model where radio counterparts could be seen at ∼1 Gpc distances. We note that we are extrapolating the properties of all giant magnetar flares from a total sample of three and that it is impossible to yet know what other subclasses of magnetar hyperflares might actually exist. Another issue with the theory is that, based on constraints from the DM, optical depth, and expansion of the supernova (SN) ejecta surrounding the magnetar, the age of the source must be less than 100 yr (Metzger et al. 2017; Murase et al. 2016). This implies that as the remnant expands in time we should expect to see the observed DM evolve as well, despite there being no such evidence for this based on the DM of the repeating bursts from FRB 121102. However, given these caveats we still consider the theory that FRBs originate as magnetar hyperflares as plausible.

[12] *K*-corrections allow a conversion between a measurement at a redshift, z, to its equivalent rest-frame value.

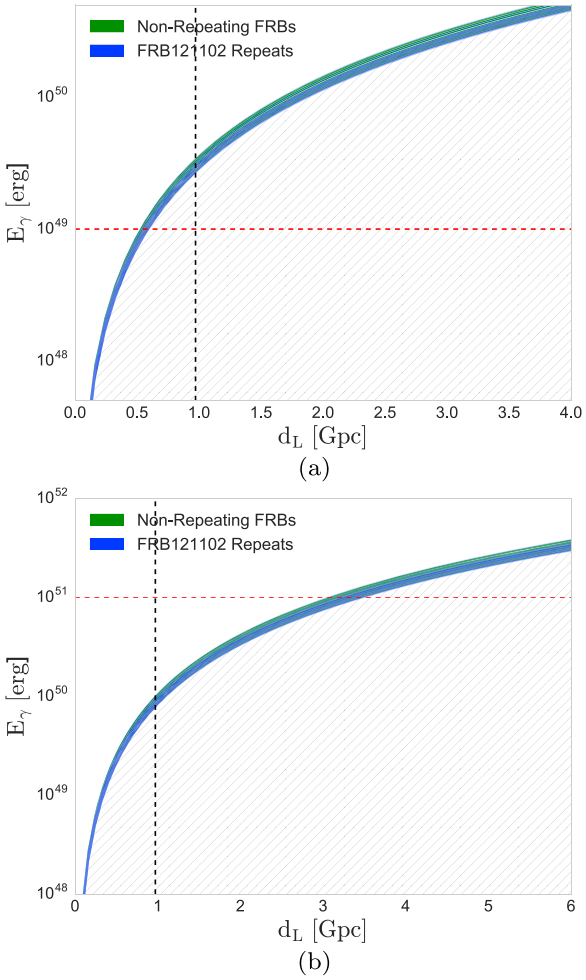

Figure 1. Given the fluence upper limits on varying timescales (Table 1) we can predict how far away FRBs can be observed as predicted by different models. The hatched pattern represents viable parameter space. The black dashed line is the reported distance of the host galaxy of FRB 121102. (a) The red dashed line represents the energy cutoff for magnetar hyperflares ($E_\gamma < 10^{49}$ erg). (b) The red dashed line represents the energy cutoff for coalescence models ($E_\gamma < 10^{51}$ erg).

3.2.3. Coalescence Models

Dokuchaev & Eroshenko (2017) proposed a model where FRBs are caused by collisions between neutron stars in the centers of evolved galaxies. This coalescence is suggested to generate short GRBs and the extreme energies produced have led some to suggest they could also power FRBs (Berger 2014; Takami et al. 2014). The model predicts that a binary merger is not necessary to generate an FRB signal. As the neutron stars inspiral, their magnetic fields become synchronized with the binary rotation. This can result in magnetic reconnections that produce coherent radio emission.

The inferred rate of FRBs is much higher than that of neutron star–neutron star mergers. Only the most optimistic binary neutron star merger rates could begin to compare with the lowest expected FRB rates (Callister et al. 2016). Assuming this is the case, however, would imply that the majority of binary neutron star mergers will result in an observable FRB. This is in apparent conflict with the small number of known FRBs—only 70 to date (FRBCAT)—and the lack of any associated FRB with the recent GRB 170817A/GW170817 event (Abbott et al. 2017a). However, we caution that radio observations of GW170817 did not begin until approximately 12 hr after the merger, making firm conclusions difficult to draw.

With the notable exception of GRB 170817A (a highly subluminous event; Abbott et al. 2017b), the prompt isotropic energy release of short GRBs is $\sim 10^{51}$–10^{52} erg (Berger 2014). The divide between short and long GRBs occurs at about 2 s (Kouveliotou et al. 1993), therefore we consider timescales of high-energy emission of 1 s. We take a similar approach to the magnetar model and constrain distances out to which we should expect to see FRBs if they are powered by coalescence (Figure 1). We find that colliding neutron stars must reside outside of ~3 Gpc to account for the lack of detected high-energy emission we observe. This is inconsistent with the FRB 121102 result and the observed DMs of the other FRBs. If we attribute all of the observed DM to propagation through the IGM then we would expect FRBs to reside at distances of no more than ~3 Gpc (Thornton et al. 2013). In addition, low-luminosity, GRB 170817A-like events must be located at distances further than a few hundred Mpc to account for a lack of radio emission. This is inconsistent with the merger's reported distance of only 40 Mpc (Abbott et al. 2017a).

If FRBs are the result of collisions between neutron stars, then the absence of gamma-ray emission is puzzling. Dokuchaev & Eroshenko (2017) proposed that the GRB occurred off-axis and we are left seeing only the radio afterglow. In addition, they propose that collisions of this kind may also produce relativistic fireballs that can be lensed by the central supermassive black hole. The effects of this lensing are to produce a range of achromatic flashes of varying wavelengths. In this case the gas produced by the collision could absorb some of the high-energy emission. However, given the inconsistencies between this model and the FRB rate, observed FRB DMs, and the distances of the Repeater and GRB 170817A we consider it unlikely that FRBs are caused by binary neutron star mergers.

3.2.4. "Cosmic Combs"

Zhang (2017) proposed a model that can reproduce the variety of observations associated with FRBs (e.g., the gamma-ray signal associated with FRB 131104, the active galactic nucleus (AGN) possibly coincident with FRB 150418,[13] and the repeating nature of FRB 121102). The magnetosphere of a cosmological pulsar can be "combed" by a passing astrophysical plasma stream and accelerated by magnetic reconnections to produce an FRB. The origins of the plasma stream will determine what signatures are detected. For example, Zhang proposed that the radio flare associated with the FRB 150418 event is in fact the original plasma stream, which combed a pulsar to create the observed FRB. Also, they suggested that the repeater could be powered by irregular emission from a supernova remnant. Anything from AGNs, GRBs, SNe, tidal disruption events, or stellar flares could be responsible for combing these signals from pulsars. The only condition needed to produce such a phenomenon is that the ram pressure of the plasma stream from these objects exceed the magnetic pressure of the magnetosphere of the pulsar.

Similar to Section 3.2.3, we consider the proposition that FRBs are caused by short GRBs originating from binary neutron star collisions. If we consider FRBs as counterparts to combed GRB signals then we can use a statistical approach to determine the maximum percentage of events that must come from GRB-like sources in order to account for the observed high-energy non-detections. We assume a binomial distribution of cosmic comb outcomes where p is the probability of a cosmic comb event originating from a GRB and take our sample size to be the $n = 12$ non-repeating FRBs in Table 1. Therefore, the probability of getting k observed high-energy events is

$$P = \binom{n}{k} p^k (1 - p)^{n-k}. \quad (1)$$

Because we report no significant high-energy counterparts, the probability of getting $k = 0$ events is $<17.5\%$ (at 90% confidence). If instead we calculate the probability of finding $k = 0$ events over all observations (both repeating and non-repeating, $n = 30$) then this decreases to $<7.4\%$. Therefore, we disfavor GRB cosmic combs as a plausible explanation for the origins of FRBs.

3.2.5. Other Compact Object Models

To date, there exist dozens of theories in the literature describing FRB origins. In this section we summarize additional models involving compact objects, which we feel do not warrant the full analytical treatment exhibited in previous sections.

FRBs could be produced by collapsing supramassive neutron stars (Falcke & Rezzolla 2014; Zhang 2014). While the timescale of collapse is consistent with that of FRBs, it fails to explain any repeating phenomena or the production of the radio emission itself. Similar to Section 3.2.3, binaries involving neutron stars and white dwarfs have been proposed (Gu et al. 2016; Lin et al. 2018), although they are specifically invoked to explain only the Repeater. Several models exist involving neutron star interactions with black holes (Bhattacharyya 2017; Abramowicz et al. 2018), black hole interactions with white dwarfs (Li et al. 2018), and events from various other types of black holes and AGNs (Zhang 2016; Vieyro et al. 2017), but these theories all remain highly speculative. In parallel with Section 3.2.2, it is also proposed that magnetars could instead power FRB-like signals via twists within the magnetosphere caused by crustal slippage (Wadiasingh & Timokhin 2019).

For a full treatment of all plausible theories on FRB origins we direct the reader to recent reviews, which cover models involving both compact and non-compact sources (Katz 2018; Lorimer 2018).

4. Conclusions

We searched for high-energy counterparts to FRBs in *Fermi* GBM, *Fermi* LAT, and *Swift* BAT. We detect no significant high-energy emission on timescales of several 0.1–100 s. We report upper limits to the emission in Table 1 for each timescale (0.1, 1, 10, and 100 s) and energy range (15–350, 300–40,000 keV, and

[13] Keane (2016) used the coincidence of FRB 150418 to a fading radio transient to identify a host galaxy at $z \sim 0.5$. Williams & Berger (2016) claimed that the radio source is instead AGN variability and is not connected to the FRB.

60–100,000 MeV) and also report limits on the ratio of radio to high-energy fluence for timescales of 0.1 and 100 s (Table 2).

We consider the implications of non-detections in the context of several theoretical models. We regard the neutron star coalescence model as highly unlikely, as it is inconsistent with the observed FRB DMs, the number of observed FRBs to date, and the distance of the FRB 121102 host galaxy. In addition, if the cosmic comb model explains FRBs then it is unlikely that FRBs are caused by GRBs "combing" pulsars.

Two of the more promising theories—magnetically or rotationally powered neutron stars—remain viable. We place lower limits on the distance for magnetar hyperflares, which are consistent with the observed FRB DMs and the FRB 121102 result. While the non-detection of high-energy emission agrees with the rotationally powered theory, it does not agree with the distance of the repeater.

Although we exclude FRB 131104 due to its low partial coding fraction, we compare our results from the other FRBs with the results of its claimed counterpart in BAT (DeLaunay et al. 2016). If FRBs are caused by events similar to that reported by DeLaunay, then for the majority of our sample the observed gamma-ray fluence should have been larger than reported here.

As this paper was being written new FRBs have been reported, including the second repeating burst FRB 180814.J0422+73 (see the FRB Catalog at frbcat.org Petroff et al. 2016). We will continue to explore the high-energy properties of these (and any other future FRBs) with the same methods described in this paper. However, for the best results a dedicated, multi-wavelength follow-up procedure needs to be put in place. Ideally, there would exist a joint campaign between telescopes for co-observing candidates so that data at other wavelengths would be immediately available. If there are in fact no counterparts to FRBs at other wavelengths, then future progress in the field will require precise localization from radio measurements, in particular interferometry.

We thank the anonymous referee for their constructive comments, which improved the quality of the manuscript. The *Fermi* LAT Collaboration acknowledges generous ongoing support from a number of agencies and institutes that have supported both the development and the operation of the LAT as well as scientific data analysis. These include the National Aeronautics and Space Administration and the Department of Energy in the United States, the Commissariat à l'Energie Atomique and the Centre National de la Recherche Scientifique/Institut National de Physique Nucléaire et de Physique des Particules in France, the Agenzia Spaziale Italiana and the Istituto Nazionale di Fisica Nucleare in Italy, the Ministry of Education, Culture, Sports, Science and Technology (MEXT), High Energy Accelerator Research Organization (KEK) and Japan Aerospace Exploration Agency (JAXA) in Japan, and the K. A. Wallenberg Foundation, the Swedish Research Council and the Swedish National Space Board in Sweden.

Additional support for science analysis during the operations phase is gratefully acknowledged from the Istituto Nazionale di Astrofisica in Italy and the Centre National d'Études Spatiales in France. This work performed in part under DOE Contract DE-AC02-76SF00515.

Appendix

A.1. FRB Observations by Instrument

Table 3 summarizes which FRBs were observable within the FOV of the *Fermi* GBM, *Fermi* LAT, and *Swift* BAT at the time of radio detection. Here, Y denotes the FRB was observed by the instrument and N denotes it was not observed. The subsequent repeating bursts from FRB 121102 have been combined for brevity. FRB 131104 was detected on the edge of the BAT FOV but is excluded due to its low partial coding fraction.

A.2. Summary of Extraneous Signals Detected with the Fermi GBM Targeted Search

We follow a similar approach in our *Fermi* GBM analysis to that of electromagnetic follow-up of gravitational-wave compact binary sources. Blackburn et al. (2015) developed a Bayesian method to search GBM continuous data for coincident signals around LIGO triggers. The analysis only requires an event time for the LIGO trigger and a localization probability map. Therefore it is convenient to adapt the method to our purposes for candidates temporally coincident with FRBs. A log likelihood-ratio (log LR) parameter is calculated for each FRB in the *Fermi* GBM data to determine the probability of the presence of a signal compared to the null hypothesis of a constant background (see Goldstein et al. 2016 for more details about this analysis). LogLR values greater than 10.0 are likely indicative of a real signal. We find six candidate signals coincident in time with the FRB detections ($t_{\rm FRB}$); however, we determine them all to be unrelated for the reasons outlined below:

Table 3
Summary of Observations Available per FRB

FRB Name	*Fermi* GBM	*Fermi* LAT	*Swift* BAT
010125	N	N	N
010621	N	N	N
010724	N	N	N
090625	Y	Y	N
110220	N	N	N
110523	Y	N	N
110626	Y	N	N
110703	Y	N	N
120127	N	N	N
121002	N	N	N
121102	Y	Y	N
130626	N	N	N
130628	Y	Y	N
130729	Y	N	N
131104	Y	N	N
140514	N	N	N
150215	Y	Y	Y
150418	Y	Y	N
150807	Y	N	N
160317	Y	Y	N
160410	N	N	Y
160608	Y	Y	N
170107	N	N	N

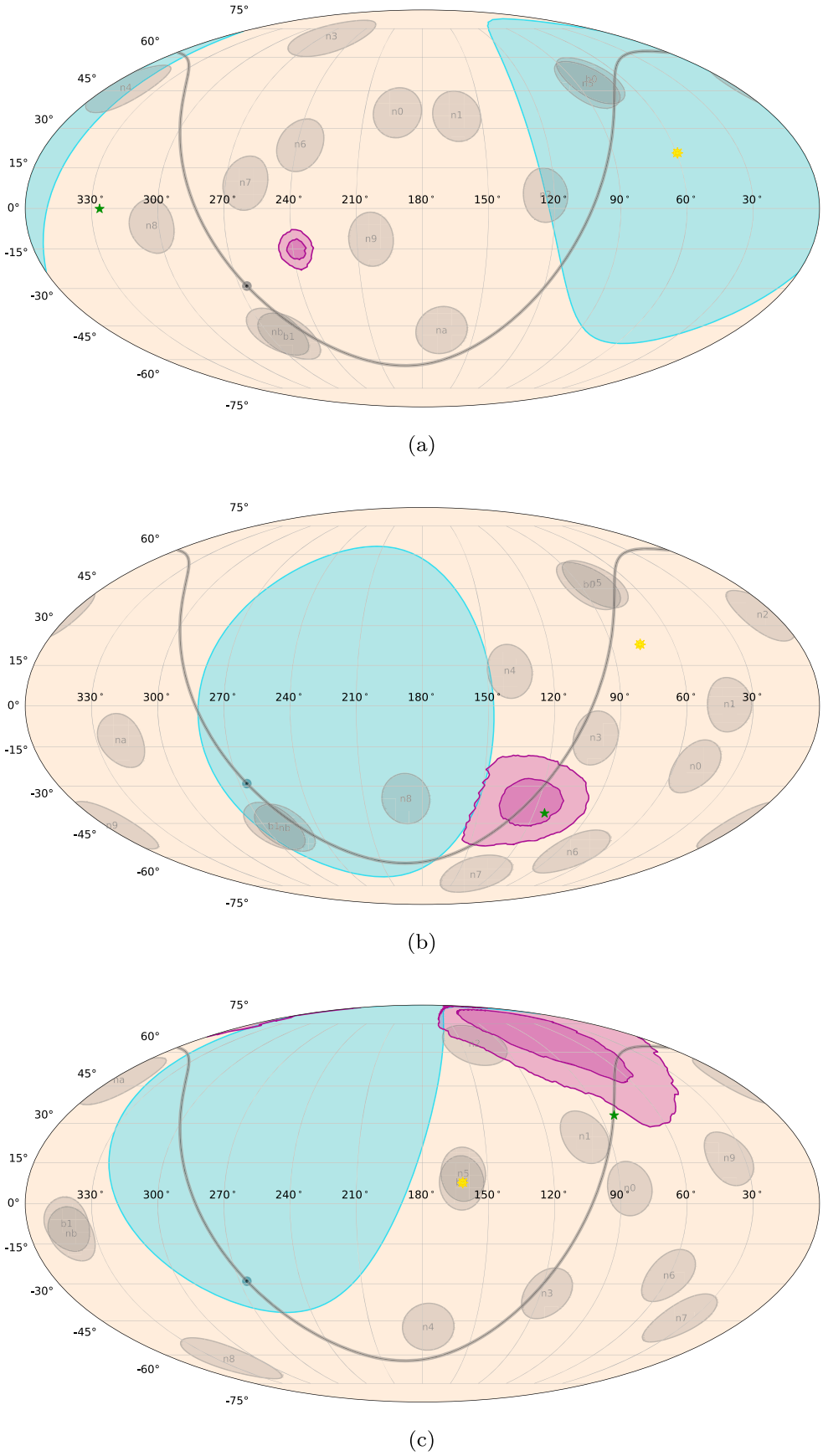

Figure 2. Localization map of the candidate signal for (a) FRB 110523, (b) FRB 160608, and (c) FRB 121102 Burst 19. The blue shaded region represents the area occulted by the Earth, the gray stripe is the Galactic plane, the gray circles represent the positions of each of the detectors, and the yellow and green stars are the locations of the Sun and FRB, respectively. The purple region shows the 50% and 90% confidence regions for the GBM localization of the candidate signal.

A.2.1. Local Particle Activity

Fermi is sensitive to increased levels of local particle activity in the magnetosphere along its orbit (even when outside the SAA). These events are characterized by long (several tens to hundreds of seconds), smooth, and hard signals observed as a slow rise against the normal background emission. Three of the candidate signals (FRB 131104 and bursts 19 and 20 from FRB 121102) discovered by the targeted search are likely caused by this local magnetospheric activity. All three were identified within the 100 s timescale searches with log LR values greater than 10.0. None of the signals are temporally coincident with the FRBs. The signal around burst 19 occurred 90 s before $t_{\rm FRB}$, the signal around burst 20 occurred 450 s before $t_{\rm FRB}$, and a third signal occurred 331 s after the $t_{\rm FRB}$ of FRB 131104. We considered all three candidate signals to be unrelated.

A.2.2. Other Unrelated Signals

FRB 110523: only CTIME data are available for the analysis of FRB 110523. A candidate signal is seen ∼80 s before $t_{\rm FRB}$ with a duration of 8 s and a log LR of 22. The signal is soft and localizes near, but not on, the Galactic plane (Figure 2(a)). The signal is not localized near the FRB. We assume this to be unrelated particle activity.

FRB 160608: a candidate signal is seen ∼10 s before $t_{\rm FRB}$ with a log LR of 10.8. The signal properties are consistent with that of a Galactic transient (i.e., a soft, 10 s long burst that localizes to the Galactic plane). Although the localization is consistent with the FRB (Figure 2(b)) based on further analysis with the BAT we suspect it is likely a flare from the nearby high-mass X-ray binary system Vela X-1.

FRB 121102 Burst 19: a second candidate signal is seen in addition to the local particle activity described above. A shorter event occurs 109 s before $t_{\rm FRB}$ for a duration of 10 s with a log LR of 13.6. However, given the disagreement with the FRB location (Figure 2(c)) and the number of trials, we consider this signal both insignificant and unrelated.

ORCID iDs

Virginia Cunningham https://orcid.org/0000-0003-2292-0441
S. Bradley Cenko https://orcid.org/0000-0003-1673-970X
Adam Goldstein https://orcid.org/0000-0002-0587-7042
Judith Racusin https://orcid.org/0000-0002-4744-9898

References

Abbott, B. P., Abbott, R., Abbott, T. D., et al. 2017a, ApJL, 848, L12
Abbott, B. P., Abbott, R., Abbott, T. D., et al. 2017b, ApJL, 848, L13
Abramowicz, M. A., Bejger, M., & Wielgus, M. 2018, ApJ, 868, 17
Acero, F., Ackermann, M., Ajello, M., et al. 2015, ApJS, 218, 23
Ackermann, M., Ajello, M., Albert, A., et al. 2012, ApJS, 203, 4
Ackermann, M., Ajello, M., Albert, A., et al. 2016, ApJL, 823, L2
Arnaud, K. A. 1996, in ASP Conf. Ser. 101, Astronomical Data Analysis Software and Systems V, ed. G. H. Jacoby & J. Barnes (San Francisco, CA: ASP), 17
Atwood, W. B., Abdo, A. A., Ackermann, M., et al. 2009, ApJ, 697, 1071
Band, D., Matteson, J., Ford, L., et al. 1993, ApJ, 413, 281
Barthelmy, S. D., Barbier, L. M., Cummings, J. R., et al. 2005, SSRv, 120, 143
Berger, E. 2014, ARA&A, 52, 43
Bhattacharyya, S. 2017, arXiv:1711.09083
Blackburn, L., Briggs, M. S., Camp, J., et al. 2015, ApJS, 217, 8
Bregman, J. N. 2007, ARA&A, 45, 221
Buehler, R., Scargle, J. D., Blandford, R. D., et al. 2012, ApJ, 749, 26
Bühler, R., & Blandford, R. 2014, RPPh, 77, 066901
Callister, T., Kanner, J., & Weinstein, A. 2016, ApJL, 825, L12
Champion, D. J., Petroff, E., Kramer, M., et al. 2016, MNRAS, 460, L30
Chatterjee, S., Law, C. J., Wharton, R. S., et al. 2017, Natur, 541, 58
Connaughton, V., Briggs, M. S., Goldstein, A., et al. 2015, ApJS, 216, 32
Cordes, J. M., & Lazio, T. J. W. 2002, arXiv:astro-ph/0207156
Cordes, J. M., & Wasserman, I. 2016, MNRAS, 457, 232
DeLaunay, J. J., Fox, D. B., Murase, K., et al. 2016, ApJL, 832, L1
Dokuchaev, V. I., & Eroshenko, Y. N. 2017, arXiv:1701.02492
Duncan, R. C., & Thompson, C. 1992, ApJL, 392, L9
Falcke, H., & Rezzolla, L. 2014, A&A, 562, A137
Gehrels, N., Chincarini, G., Giommi, P., et al. 2004, ApJ, 611, 1005
Goldstein, A., Burns, E., Hamburg, R., et al. 2016, arXiv:1612.02395
Gu, W.-M., Dong, Y.-Z., Liu, T., Ma, R., & Wang, J. 2016, ApJL, 823, L28
Hankins, T. H., & Eilek, J. A. 2007, ApJ, 670, 693
Hurley, K., Boggs, S. E., Smith, D. M., et al. 2005, Natur, 434, 1098
Hurley, K., Cline, T., Mazets, E., et al. 1999, Natur, 397, 41
Katz, J. I. 2018, PrPNP, 103, 1
Keane, E. F. 2016, MNRAS, 459, 1360
Keane, E. F., & Petroff, E. 2015, MNRAS, 447, 2852
Kouveliotou, C., Dieters, S., Strohmayer, T., et al. 1998, Natur, 393, 235
Kouveliotou, C., Meegan, C. A., Fishman, G. J., et al. 1993, ApJL, 413, L101
Krimm, H. A., Holland, S. T., Corbet, R. H. D., et al. 2013, ApJS, 209, 14
Kulkarni, S. R., Ofek, E. O., & Neill, J. D. 2015, arXiv:1511.09137
Li, L.-B., Huang, Y.-F., Geng, J.-J., & Li, B. 2018, RAA, 18, 061
Li, W., Chornock, R., Leaman, J., et al. 2011, MNRAS, 412, 1473
Lien, A., Sakamoto, T., Gehrels, N., et al. 2014, ApJ, 783, 24
Lin, Y., Cheng, Z., & Gan, L. 2018, SSPMA, 48, 029501
Lorimer, D. R. 2018, NatAs, 2, 860
Lorimer, D. R., Bailes, M., McLaughlin, M. A., Narkevic, D. J., & Crawford, F. 2007, Sci, 318, 777
Lyubarsky, Y. 2014, MNRAS, 442, L9
Lyutikov, M. 2002, ApJL, 580, L65
Manchester, R. N., Hobbs, G. B., Teoh, A., & Hobbs, M. 2005, AJ, 129, 1993
Maoz, D., Loeb, A., Shvartzvald, Y., et al. 2015, MNRAS, 454, 2183
Marcote, B., Paragi, Z., Hessels, J. W. T., et al. 2017, ApJL, 834, L8
Mazets, E. P., Golentskii, S. V., Ilinskii, V. N., Aptekar, R. L., & Guryan, I. A. 1979, Natur, 282, 587
McQuinn, M. 2014, ApJL, 780, L33
Meegan, C., Lichti, G., Bhat, P. N., et al. 2009, ApJ, 702, 791
Metzger, B. D., Berger, E., & Margalit, B. 2017, ApJ, 841, 14
Mickaliger, M. B., McLaughlin, M. A., Lorimer, D. R., et al. 2012, ApJ, 760, 64
Murase, K., Kashiyama, K., & Mészáros, P. 2016, MNRAS, 461, 1498
Nicholl, M., Williams, P. K. G., Berger, E., et al. 2017, ApJ, 843, 84
Palaniswamy, D., Li, Y., & Zhang, B. 2018, ApJL, 854, L12
Palmer, D. M., Barthelmy, S., Gehrels, N., et al. 2005, Natur, 434, 1107
Pen, U.-L., & Connor, L. 2015, ApJ, 807, 179
Petroff, E., Barr, E. D., Jameson, A., et al. 2016, PASA, 33, e045
Popov, S. B., & Postnov, K. A. 2013, arXiv:1307.4924
Readhead, A. C. S. 1994, ApJ, 426, 51
Savchenko, V., Ferrigno, C., Panessa, F., et al. 2018a, ATel, 11431, 1
Savchenko, V., Ferrigno, C., Panessa, F., et al. 2018b, ATel, 11387, 1
Savchenko, V., Panessa, F., Ferrigno, C., et al. 2018c, ATel, 11386, 1
Scholz, P., Bogdanov, S., Hessels, J. W. T., et al. 2017, ApJ, 846, 80
Scholz, P., Spitler, L. G., Hessels, J. W. T., et al. 2016, ApJ, 833, 177
Shull, J. M., Smith, B. D., & Danforth, C. W. 2012, ApJ, 759, 23
Spitler, L. G., Scholz, P., Hessels, J. W. T., et al. 2016, Natur, 531, 202
Striani, E., Tavani, M., Piano, G., et al. 2011, ApJL, 741, L5
Takami, H., Kyutoku, K., & Ioka, K. 2014, PhRvD, 89, 063006
Tendulkar, S. P., Bassa, C. G., Cordes, J. M., et al. 2017, ApJL, 834, L7
Tendulkar, S. P., Kaspi, V. M., & Patel, C. 2016, ApJ, 827, 59
The CHIME/FRB Collaboration, Amiri, M., Bandura, K., et al. 2019, Natur, 566, 235
Thornton, D., Stappers, B., Bailes, M., et al. 2013, Sci, 341, 53
Vieyro, F. L., Romero, G. E., Bosch-Ramon, V., Marcote, B., & del Valle, M. V. 2017, A&A, 602, A64
Wadiasingh, Z., & Tomkhin, A. 2019, arXiv:1904.12036
Williams, P. K. G., & Berger, E. 2016, ApJL, 821, L22
Yamasuki, S., Totani, T., & Kawanaka, N. 2016, MNRAS, 460, 2875
Zhang, B. 2014, ApJL, 780, L21
Zhang, B. 2016, ApJL, 827, L31
Zhang, B. 2017, ApJL, 836, L32
Zhou, B., Li, X., Wang, T., Fan, Y.-Z., & Wei, D.-M. 2014, PhRvD, 89, 107303